Phase behavior of shape-changing spheroids

P. I. C. Teixeira[1,2,*] and A. J. Masters[3]
[1]*ISEL–Instituto Superior de Engenharia de Lisboa, Instituto Politécnico de Lisboa, Rua Conselheiro Emídio Navarro 1, 1959-007 Lisbon, Portugal*
[2]*Centro de Física Teórica e Computacional, Faculdade de Ciências, Universidade de Lisboa, Campo Grande, Edifício C8, 1749-016 Lisbon, Portugal*
[3]*School of Chemical Engineering and Analytical Science, University of Manchester, Manchester M60 1QD, United Kingdom*
(Received 10 April 2015; revised manuscript received 14 September 2015; published 4 December 2015)

We introduce a simple model for a biaxial nematic liquid crystal. This consists of hard spheroids that can switch shape between prolate (rodlike) and oblate (platelike) subject to an energy penalty $\Delta\epsilon$. The spheroids are approximated as hard Gaussian overlap particles and are treated at the level of Onsager's second-virial description. We use both bifurcation analysis and a numerical minimization of the free energy to show that, for *additive* particle shapes, (i) there is no stable biaxial phase even for $\Delta\epsilon = 0$ (although there is a metastable biaxial phase in the same density range as the stable uniaxial phase) and (ii) the isotropic-to-nematic transition is into either one of two degenerate uniaxial phases, rod rich or plate rich. We confirm that even a small amount of shape nonadditivity may stabilize the biaxial nematic phase.

DOI: 10.1103/PhysRevE.92.062506 PACS number(s): 64.70.mf, 61.30.Cz

I. INTRODUCTION

Basic stripped-down models of low-molecular-weight liquid crystals treat them as collections of either hard rods or hard plates. However, small, flexible molecules known as tetrapodes also exhibit liquid crystalline phases, including the elusive biaxial nematic phase [1,2]. This is a consequence of the interplay between conformational and packing entropies: the molecules are able to adopt an anisometric stable conformation that allows them to pack more efficiently into orientationally ordered mesophases. Previous theoretical studies of such systems have been presented [3–5]. In particular, Vanakaras and coworkers [3,4] introduced a model of interconverting hard rods and plates and showed that, at the level of the L2 approximation of Onsager theory, it does not exhibit any biaxial behavior. Mixtures of prolate and oblate spheroids [6] do, nevertheless, appear to exhibit a stable biaxial nematic phase when treated with the full Onsager theory, which is confirmed by computer simulation [6]. It is therefore of interest to investigate interconverting spheroids, for which it may be important to solve the full Onsager theory rather than make the L2 approximation. We will introduce a minimal model which permits a clear, detailed analysis, for which we can compare the L2 and full Onsager approaches.

The remainder of this paper is organized as follows: in Sec. II we describe our model and the simple Onsager theory used to study it. Our results are presented in Sec. III: as a prerequisite to applying the theory to our chosen model, we derive an analytic expression for the angle-dependent excluded volume of two unlike particles (Sec. III A). We then perform a bifurcation analysis of the stability of the isotropic phase with respect to the (uniaxial or biaxial) nematic phase (Sec. III B). Finally, the order parameters, pressure, and Gibbs potential of the uniaxial and biaxial phases are calculated, first using the L2 approximation (Sec. III C) and then fully numerically (Sec. III D). The effect of shape nonadditivity is also investigated. Conclusions and directions for future work are collected in Sec. IV.

II. THEORY

A. Theory and model

In our model, which is closely related to that of Vanakaras *et al.* [3,4], a particle can exist in one of two states: a prolate and an oblate spheroid. The energies of these two states (conformers) differ by a prescribed amount $\Delta\epsilon$, and the two states are in chemical equilibrium [3,4]. The Helmholtz free energy density (FED) of a uniform mixture of interconverting rods (R) and plates (P) of densities ρ_R and ρ_P is, in the Onsager second-virial approximation,

$$\begin{aligned}\beta f(\rho_R,\rho_P) = {}& \rho_R[\log(\Lambda^3\rho_R) - 1] + \rho_P[\log(\Lambda^3\rho_P) - 1] \\ & + \rho_R \int \hat{f}_R(\omega)\log[4\pi\,\hat{f}_R(\omega)]d\omega \\ & + \rho_P \int \hat{f}_P(\omega)\log[4\pi\,\hat{f}_P(\omega)]d\omega \\ & + \rho_R^2 \int \hat{f}_R(\omega_1)B_{RR}(\omega_1,\omega_2)\hat{f}_R(\omega_2)\,d\omega_1 d\omega_2 \\ & + \rho_P^2 \int \hat{f}_P(\omega_1)B_{PP}(\omega_1,\omega_2)\hat{f}_P(\omega_2)\,d\omega_1 d\omega_2 \\ & + 2\rho_R\rho_P \int \hat{f}_R(\omega_1)B_{RP}(\omega_1,\omega_2)\hat{f}_P(\omega_2)\,d\omega_1 d\omega_2 \\ & + \epsilon_R\rho_R + \epsilon_P\rho_P, \end{aligned} \tag{1}$$

where $\beta = 1/k_BT$, $B_{ij}(\omega_1,\omega_2)$ $(i,j = R,P)$ are the orientational second-virial coefficients, $\hat{f}_R(\omega)$ $[\hat{f}_P(\omega)]$ is the orientational distribution function (ODF) of rods (plates), and ϵ_R (ϵ_P) is the energy penalty (here and henceforth in units of k_BT) associated with a rod (plate). The chemical potentials (to within an additive constant) of rods and plates are easily

*Corresponding author: piteixeira@fc.ul.pt

found:

$$\beta\mu_R = \log\rho_R + \int \hat{f}_R(\omega)\log[4\pi\hat{f}_R(\omega)]d\omega + 2\rho_R\int \hat{f}_R(\omega_1)B_{RR}(\omega_1,\omega_2)\hat{f}_R(\omega_2)\,d\omega_1 d\omega_2 + 2\rho_P\int \hat{f}_R(\omega_1)B_{RP}(\omega_1,\omega_2)\hat{f}_P(\omega_2)\,d\omega_1 d\omega_2 + \epsilon_R, \tag{2}$$

$$\beta\mu_P = \log\rho_P + \int \hat{f}_P(\omega)\log[4\pi\hat{f}_P(\omega)]d\omega + 2\rho_P\int \hat{f}_P(\omega_1)B_{PP}(\omega_1,\omega_2)\hat{f}_P(\omega_2)\,d\omega_1 d\omega_2 + 2\rho_R\int \hat{f}_R(\omega_1)B_{RP}(\omega_1,\omega_2)\hat{f}_P(\omega_2)\,d\omega_1 d\omega_2 + \epsilon_P. \tag{3}$$

Likewise, the ODFs of rods and plates are obtained by functionally differentiating the FED subject to the normalization constraints:

$$\frac{\delta(\beta f)}{\delta\hat{f}_R(\omega)} = \rho_R\lambda_R$$

$$\Rightarrow \hat{f}_R(\omega) = C_R^{-1}\exp\left[-2\rho_R\int B_{RR}(\omega,\omega')\hat{f}_R(\omega')\,d\omega' - 2\rho_P\int B_{RP}(\omega,\omega')\hat{f}_P(\omega')\,d\omega'\right], \tag{4}$$

$$\frac{\delta(\beta f)}{\delta\hat{f}_P(\omega)} = \rho_P\lambda_P$$

$$\Rightarrow \hat{f}_P(\omega) = C_P^{-1}\exp\left[-2\rho_P\int B_{PP}(\omega,\omega')\hat{f}_P(\omega')\,d\omega' - 2\rho_R\int B_{RP}(\omega,\omega')\hat{f}_R(\omega')\,d\omega'\right], \tag{5}$$

where C_R and C_P are normalization constants and we have written the Lagrange multipliers for rods (plates) as $\rho_R\lambda_R$ ($\rho_P\lambda_P$) for convenience.

Equating the chemical potentials, Eqs. (2) and (3), and using Eqs. (4) and (5) yield

$$\frac{\rho_R}{\rho_P} = \frac{C_P}{C_R}\exp[-(\epsilon_R-\epsilon_P)] = \frac{C_P}{C_R}\exp(-\Delta\epsilon), \tag{6}$$

where $\Delta\epsilon = \epsilon_R - \epsilon_P$. Because the total density is

$$\rho = \rho_R + \rho_P, \tag{7}$$

we find, for the equilibrium densities of rods and plates,

$$\rho_R = \frac{\rho}{1+(C_P/C_R)e^{\Delta\epsilon}}, \tag{8}$$

$$\rho_P = \frac{\rho}{1+(C_R/C_P)e^{-\Delta\epsilon}}. \tag{9}$$

These equations are not closed-form relationships, as both C_R and C_P also depend on ρ_R and ρ_P. They do, however, tell us that when $\Delta\epsilon > 0$ (<0) rods (plates) cost more energy than plates (rods), and the system will be plate rich (rod rich).

The same general approach (with or without Parsons-Lee rescaling) has been successfully used to understand the phase behavior of mixtures of rodlike and platelike particles [6–11]; the difference is that here, as in [3,4], the composition is not fixed *a priori* but will depend on $\Delta\epsilon$. Thus ϵ_R and ϵ_P effectively shift the chemical potentials of rods and plates, and $\Delta\epsilon$ is directly related to the intrinsic probabilities of rods and plates as defined in [3,4].

We choose to describe the interactions of rods and plates by the simple hard Gaussian overlap (HGO) model [12] generalized to mixtures:

$$U_{ij}(\mathbf{r}_{12},\omega_1,\omega_2) = \begin{cases} 0 & \text{if } r_{12} \geqslant \sigma(\hat{\mathbf{r}}_{12},\omega_1,\omega_2), \\ \infty & \text{if } r_{12} < \sigma(\hat{\mathbf{r}}_{12},\omega_1,\omega_2), \end{cases} \tag{10}$$

where $\omega_k = (\theta_k,\phi_k)$ are the polar and azimuthal angles specifying the orientation of the long axis of particle k and $\hat{\mathbf{r}}_{12} = \mathbf{r}_{12}/r_{12}$ is a unit vector along the line connecting the centers of the two particles, either of which may be a rod or a plate (i.e., $i,j = R,P$). For like particles, the contact distance $\sigma(\hat{\mathbf{r}}_{12},\omega_1,\omega_2)$ is that originally determined by Berne and Pechukas [13], who considered the overlap of two ellipsoidal Gaussians. This was later extended to unlike particles of length l_k and breadth d_k ($k = 1,2$) by Cleaver *et al.* [14]:

$$\sigma(\hat{\mathbf{r}}_{12},\omega_1,\omega_2) = \sigma_0\left[1-\frac{1}{2}\chi\left\{\frac{(\alpha\hat{\mathbf{r}}_{12}\cdot\hat{\mathbf{u}}_1+\alpha^{-1}\hat{\mathbf{r}}_{12}\cdot\hat{\mathbf{u}}_2)^2}{1+\chi(\hat{\mathbf{u}}_1\cdot\hat{\mathbf{u}}_2)} + \frac{(\alpha\hat{\mathbf{r}}_{12}\cdot\hat{\mathbf{u}}_1-\alpha^{-1}\hat{\mathbf{r}}_{12}\cdot\hat{\mathbf{u}}_2)^2}{1-\chi(\hat{\mathbf{u}}_1\cdot\hat{\mathbf{u}}_2)}\right\}\right]^{-\frac{1}{2}}, \tag{11}$$

where $\hat{\mathbf{u}}_k = (\cos\phi_k\ \sin\theta_k, \sin\phi_k\ \sin\theta_k, \cos\theta_k)$ and

$$\sigma_0 = \sqrt{d_1^2+d_2^2}, \tag{12}$$

$$\chi = \left[\frac{(l_1^2-d_1^2)(l_2^2-d_2^2)}{(l_2^2+d_1^2)(l_1^2+d_2^2)}\right]^{1/2}, \tag{13}$$

$$\alpha^2 = \left[\frac{(l_1^2-d_1^2)(l_2^2+d_1^2)}{(l_2^2-d_2^2)(l_1^2+d_2^2)}\right]^{1/2}. \tag{14}$$

It is also useful to define the particle length-to-breadth ratio, $\kappa_k = l_k/d_k$. For like particles of moderate $\kappa \equiv \kappa_1 = \kappa_2$, the HGO model is a good approximation to the hard ellipsoid (HE) contact function [15,16], with the considerable computational advantage over HEs that $\sigma(\hat{\mathbf{r}}_{12},\omega_1,\omega_2)$, the distance of closest approach between two particles, is given in closed form.

Because HGO particles are defined in terms of their contact distance, they are "nongeometric" objects, whose volume is not well defined. In this paper we wish to suppress depletion

effects by considering rods and plates of the same volume. Therefore, following, e.g., [17], we shall approximate the volume of an HGO particle by that of a HE with the same axes lengths, i.e., $v_k = (4\pi/3) l_k d_k^2$.

B. Order parameters

Equations (4) and (5), with Eqs. (8) and (9), yield the ODFs of rods and plates, as well as their number fractions. One important question is how to identify the phase described by a pair of ODFs. Clearly, in the isotropic (I) phase, $\hat{f}_R(\omega) = \hat{f}_P(\omega) = 1/4\pi$, but how should we characterize the different N phases? These are, we recall, the rodlike (or calamitic) uniaxial phase (N_U^+), the platelike (or discotic) uniaxial phase (N_U^-), and the biaxial nematic phase (N_B). Where the distinction between the two uniaxial phases is unimportant, we shall refer to them collectively as N_U. Here we follow [6] and define the following order parameters:

$$S_R = \langle P_2(\cos\theta)\rangle_R, \tag{15}$$

$$\Delta_R = \langle \sin^2\theta \cos 2\phi\rangle_R, \tag{16}$$

$$S_P = \langle P_2(\cos\theta)\rangle_P, \tag{17}$$

$$\Delta_P = \langle \sin^2\theta \cos 2\phi\rangle_P, \tag{18}$$

where the Euler angles are measured relative to the *rod* eigenvector frame. The z axis is thus defined to be the rod director. By convention, the plates are assumed to order along the y axis of this frame. The limiting values of these order parameters are shown in Table I of [6]; these were used as initial guesses in our numerical calculations, as well as to characterize the resulting phases.

III. RESULTS

A. The second-virial coefficient of unlike HGOs

Equations (4) and (5) contain the angle-dependent second-virial coefficients of rods and plates, $B_{ij}(\omega_1,\omega_2)$ $(i,j = R,P)$. These are known for $i = j$ [18]; for $i \neq j$, this is our first original, and analytically exact, result:

$$B_{RP}(\omega_1,\omega_2) = \frac{2\pi}{3}\frac{\left[\frac{1}{2}\left(d_R^2 + d_P^2\right)\right]^{3/2}}{(1+a_{11})(1+a_{22}) - a_{12}a_{21}}, \tag{19}$$

where

$$a_{11} = \frac{c_x(1 + c_y\cos^2\theta_{12})}{1 - c_x c_y\cos^2\theta_{12}}, \tag{20}$$

$$a_{12} = \frac{c_x(1 + c_y)\cos\theta_{12}}{1 - c_x c_y\cos^2\theta_{12}}, \tag{21}$$

$$a_{21} = \frac{c_y(1 + c_x)\cos\theta_{12}}{1 - c_x c_y\cos^2\theta_{12}}, \tag{22}$$

$$a_{22} = \frac{c_y(1 + c_x\cos^2\theta_{12})}{1 - c_x c_y\cos^2\theta_{12}}, \tag{23}$$

$$c_x = \frac{d_R^2\left(1 - {\kappa'_R}^2\right)}{d_P^2 + d_R^2{\kappa'_R}^2}, \tag{24}$$

$$c_y = \frac{d_P^2\left(1 - {\kappa'_P}^2\right)}{d_R^2 + d_P^2{\kappa'_P}^2}. \tag{25}$$

The derivation of Eq. (19) is sketched in Appendix A. Additionally, shape nonadditivity may be introduced through a new parameter ν [19]:

$$\kappa'_R = \nu\kappa_R, \quad \kappa'_P = \nu^{-1}\kappa_P; \tag{26}$$

that is, a rod (plate) sees another rod (plate) with elongation κ_R (κ_P), but a rod (plate) sees a plate (rod) with elongation κ'_P (κ'_R). Varying ν changes the second-virial coefficient for two unlike particles and is known to alter the topology of the phase diagram [20].

B. Bifurcation analysis

The next step would be iteratively to solve Eqs. (4) and (5) for the ODFs, together with Eq. (8) or (9) for the density of rods or plates. However, it is useful (and physically more illuminating) first to investigate the stability of the isotropic phase relative to the uniaxial or biaxial nematic phases. This can be done analytically using bifurcation analysis and serves as a check on our later numerical work. Here we quote only the final results and refer readers to Appendix B for details.

From Eqs. (3.6) and (3.9) in [21], the overall density ρ^* at which the I phase becomes unstable with respect to either the N_U or N_B phases is

$$\rho^* = \frac{5}{4}\left[\frac{-\left(x_R^I B_{RR}^{(2)} + x_P^I B_{PP}^{(2)}\right) - \sqrt{\left(x_R^I B_{RR}^{(2)} - x_P^I B_{PP}^{(2)}\right)^2 + 4x_R^I x_P^I {B_{RP}^{(2)}}^2}}{x_R^I x_P^I\left(B_{RR}^{(2)}B_{PP}^{(2)} - {B_{RP}^{(2)}}^2\right)}\right], \tag{27}$$

where $B_{ij}^{(l)}$ are the expansion coefficients of $B_{ij}(\omega_1,\omega_2)$:

$$B_{ij}(\omega_1,\omega_2) = \sum_{l=0} B_{ij}^{(l)} P_l(\cos\theta_{12}), \tag{28}$$

$$B_{ij}^{(l)} = \frac{2l+1}{2}\int_{-1}^{+1} B_{ij}(\omega_1,\omega_2) P_l(\cos\theta_{12}) d(\cos\theta_{12}). \tag{29}$$

For hard spheroids of identical volume and $\kappa_R = 1/\kappa_P$, $B_{RR}^{(0)} = B_{PP}^{(0)} = B_{RP}^{(0)}$; that is, all the isotropic second-virial coefficients are equal. For the HGO model, $B_{RR}^{(0)} = B_{PP}^{(0)}$, but $B_{RP}^{(0)}$ differs by a small amount [see Fig. 1(a)], and this difference slightly complicates the analysis of the I phase. If, however, we make the rather good approximation that all these virial coefficients are equal (they differ by less than 3% if $\kappa \leqslant 5$), then it is

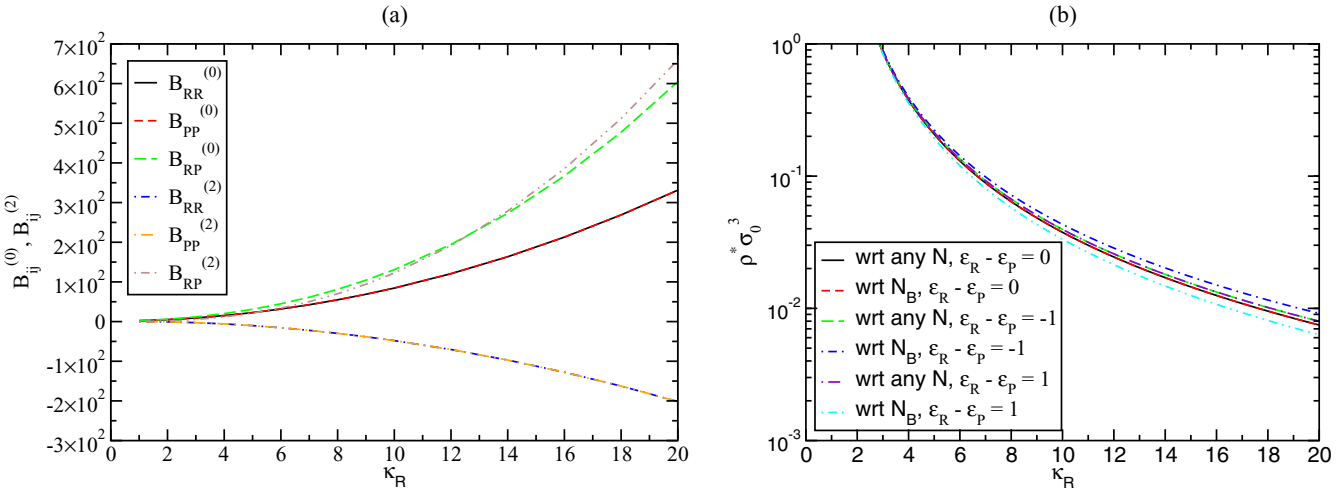

FIG. 1. (Color online) (a) Expansion coefficients $B_{ij}^{(l)}$ for $l = 0,2$. (b) Bifurcation density ρ^* of the I phase with respect to the N phase vs rod elongation κ_R for different $\Delta\epsilon = \epsilon_R - \epsilon_P$. Here $v = 1$ (additive shapes).

straightforward to calculate the number fractions of rods and plates in the I phase (where $C_R = C_P$), viz.,

$$x_R^I = \frac{e^{-\epsilon_R}}{e^{-\epsilon_R} + e^{-\epsilon_P}}, \tag{30}$$

$$x_P^I = \frac{e^{-\epsilon_P}}{e^{-\epsilon_R} + e^{-\epsilon_P}} = 1 - x_R^I. \tag{31}$$

In particular, the instability is with respect to N_B if [21, Eq. (3.19)]

$$1 + \tfrac{2}{5}\rho^*\left(x_R^I B_{RR}^{(2)} - x_P^I B_{RP}^{(2)}\right) = 0. \tag{32}$$

Here, and in the remainder of this paper, all results are for rods and plates of the same volume, such that $\kappa_P = 1/\kappa_R$; for HGO particles, this implies they also have the same excluded volume. Results for the bifurcation density are shown in Fig. 1(b): we conclude that the I phase is unstable with respect to the N_B phase if $\epsilon_R = \epsilon_P$ and with respect to the N_U phases if $\epsilon_R \neq \epsilon_P$. This, of course, does not rule out the existence of an N_B phase for $\epsilon_R \neq \epsilon_P$; it merely implies that in this case it would have to bifurcate from the N_U^+ or N_U^- phase, not from the I phase. Note that the fact that the curve for $\Delta\epsilon = 1$ lies below that for $\Delta\epsilon = 0$ does *not* mean that the I phase is unstable with respect to the N_B phase. Rather, this result is meaningless, as it predicts an instability with respect to the N_B phase at a lower density than that at which the I phase becomes unstable with respect to *any* N phase.

C. The L2 approximation

We now come back to Eqs. (4), (5), and (8) or (9). These have to be solved numerically by an iterative procedure, which is computationally difficult as good initial guesses for the ODFs are needed to achieve convergence. In order to accelerate progress, we start by resorting to the L2 approximation of Stroobants and Lekkerkerker [22]. Here the angle-dependent second-virial coefficients $B_{ij}(\omega_1,\omega_2)$ are expanded in series of Legendre polynomials as in Eqs. (28) and (29), and these expansions are truncated at order $l = 2$. Upon substitution of the truncated expansions into Eqs. (4) and (5), some of the angular integrations can be performed analytically, with the result

$$\hat{f}_R(\omega) = C_R^{-1} \exp\left\{-2\rho_R B_{RR}^{(2)}\left[P_2(\cos\theta)S_R + \tfrac{3}{4}\sin^2\theta\cos 2\phi\Delta_R\right] - 2\rho_P B_{RP}^{(2)}\left[P_2(\cos\theta)S_P + \tfrac{3}{4}\sin^2\theta\cos 2\phi\Delta_P\right]\right\}, \tag{33}$$

$$\hat{f}_P(\omega) = C_P^{-1} \exp\left\{-2\rho_P B_{PP}^{(2)}\left[P_2(\cos\theta)S_P + \tfrac{3}{4}\sin^2\theta\cos 2\phi\Delta_P\right] - 2\rho_R B_{RP}^{(2)}\left[P_2(\cos\theta)S_R + \tfrac{3}{4}\sin^2\theta\cos 2\phi\Delta_R\right]\right\}, \tag{34}$$

where we have used the definitions of the order parameters of rods and plates, Eqs. (15)–(18), as well as the spherical harmonic addition theorem. The equilibrium Helmholtz FED and chemical potentials of rods and plates, Eqs. (1)–(3), likewise become

$$\beta f(\rho_R,\rho_P) = \rho_R\left(\log\rho_R - 1 + \log\frac{4\pi}{C_R} + \epsilon_R\right) + \rho_P\left(\log\rho_P - 1 + \log\frac{4\pi}{C_P} + \epsilon_P\right) + \rho_R^2\left[B_{RR}^{(0)} - B_{RR}^{(2)}\left(S_R^2 + \frac{3}{4}\Delta_R^2\right)\right]$$
$$+ 2\rho_R\rho_P\left[B_{RP}^{(0)} - B_{RP}^{(2)}\left(S_R S_P + \frac{3}{4}\Delta_R\Delta_P\right)\right] + \rho_P^2\left[B_{PP}^{(0)} - B_{PP}^{(2)}\left(S_P^2 + \frac{3}{4}\Delta_P^2\right)\right], \tag{35}$$

$$\beta\mu_R = \log\rho_R + \log\frac{4\pi}{C_R} + 2\rho_R B_{RR}^{(0)} + 2\rho_P B_{RP}^{(0)} + \epsilon_R, \tag{36}$$

$$\beta\mu_P = \log\rho_P + \log\frac{4\pi}{C_P} + 2\rho_P B_{PP}^{(0)} + 2\rho_R B_{RP}^{(0)} + \epsilon_P, \tag{37}$$

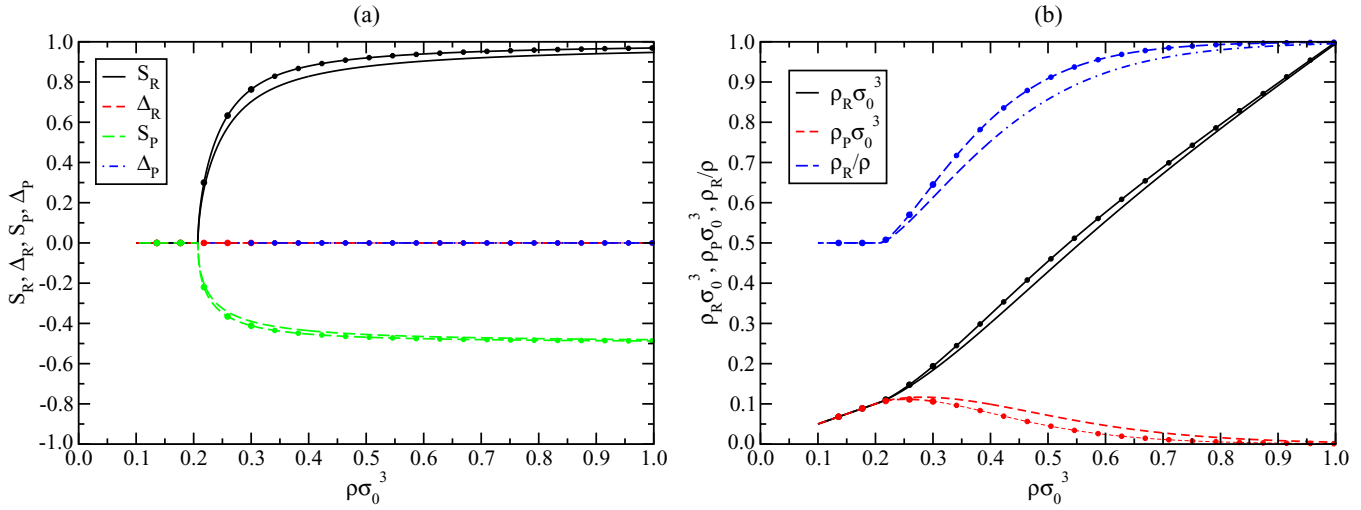

FIG. 2. (Color online) (a) Order parameters and (b) composition for the I-N_U^+ phase transition for $\kappa_R = 1/\kappa_P = 5$. $\Delta\epsilon = 0$ and $\nu = 1$. Lines without symbols: L2 approximation; lines with symbols: full numerical solution.

from which the pressure can be found via the standard thermodynamic relation

$$p = \rho_R\mu_R + \rho_P\mu_P - f. \tag{38}$$

The L2 approximation substantially reduces the computational burden, as it requires fewer numerical integrations and it is also easier to devise good initial guesses for the order parameters than for the full ODFs. This approximation is known to introduce considerable error in the description of the excluded volumes, especially for the parallel and perpendicular configurations [8]. However, as we shall see later, for our model it appears to perform reliably, for which reason it is used in many of the calculations presented henceforth.

To proceed, we equate the chemical potentials, Eqs. (36) and (37), and solve the resulting equation using NETLIB routine HYBRD, together with the self-consistency equations for the order parameters, (15)–(18). All numerical integrations were performed by 64-point Gauss-Legendre quadrature. We consider two cases: $\Delta\epsilon = 0$ (no energy penalty associated with particle shape changes) and $\Delta\epsilon \neq 0$ (one of the shapes has lower energy than the other). Recall that in all cases $\kappa_R = 1/\kappa_P$, and rods and plates have the same volume, which removes depletion effects. We also investigate the effect of shape nonadditivity, $\nu \neq 1$.

1. Unbiased shapes: $\Delta\epsilon = 0$

Depending on our initial guesses for the order parameters, we find N_U^+, N_U^-, and N_B phases (Figs. 2, 3, and 4, respectively). N_U^+ (N_U^-) is always richer in rods (plates), whereas the N_B phase is an equimolar mixture of rods and plates. The transitions, whether into the uniaxial or biaxial nematic phases, occur at the densities predicted by bifurcation analysis and, interestingly, all appear to be continuous or at least to exhibit very small density or order parameter discontinuities.

To check the relative stability of the N_U^+, N_U^-, and N_B phases we plot in Fig. 5 the Gibbs free energy per particle

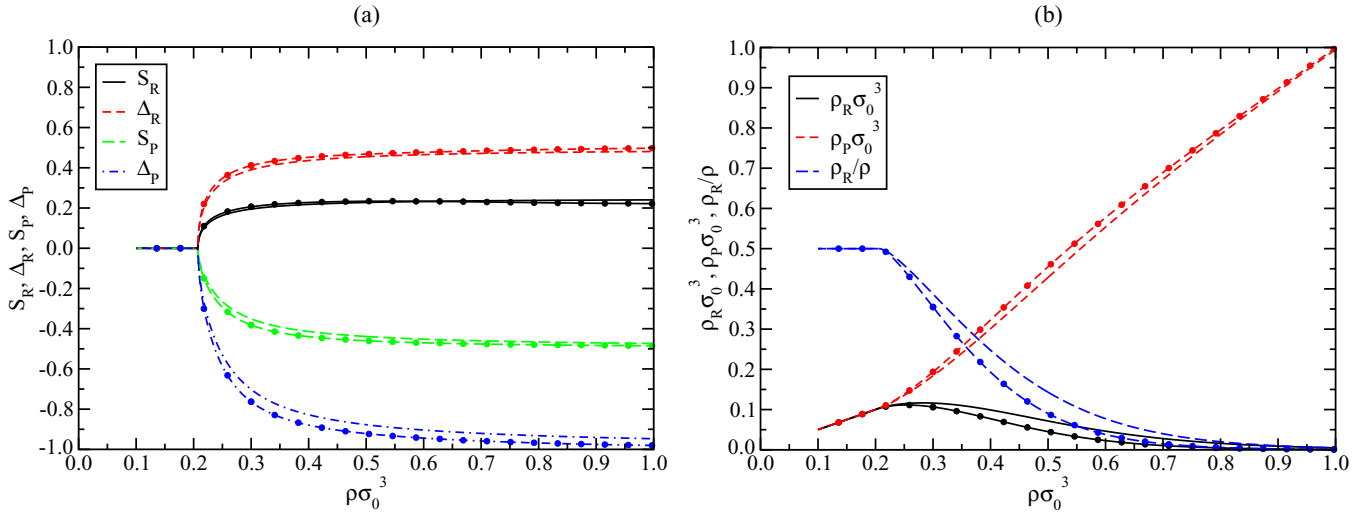

FIG. 3. (Color online) (a) Order parameters and (b) composition for the I-N_U^- phase transition for $\kappa_R = 1/\kappa_P = 5$, $\Delta\epsilon = 0$ and $\nu = 1$. Lines without symbols: L2 approximation; lines with symbols: full numerical solution.

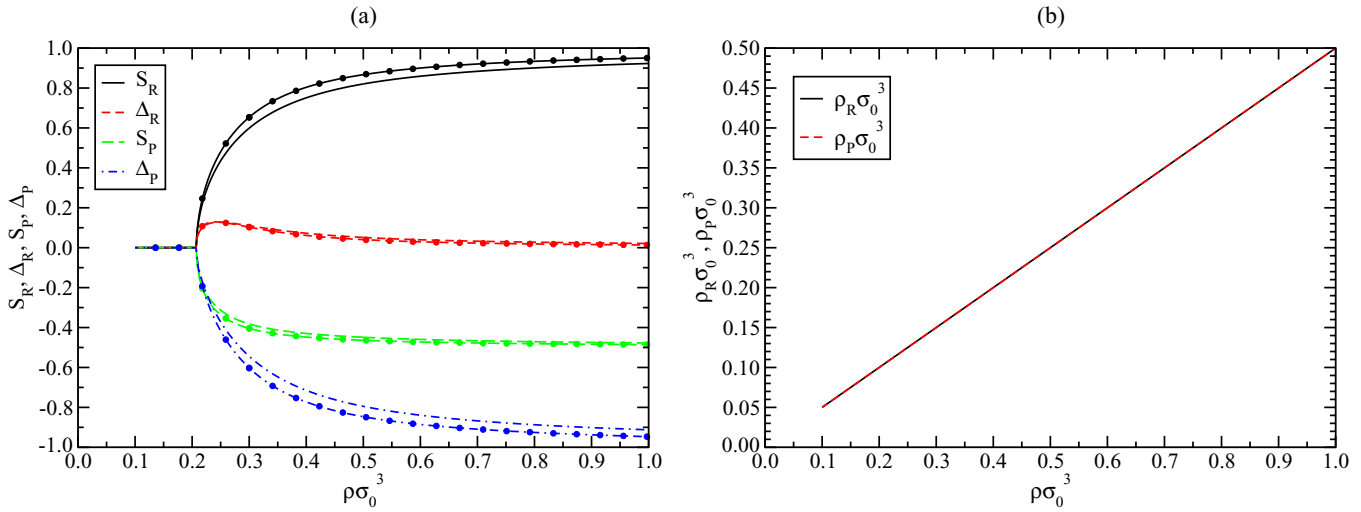

FIG. 4. (Color online) (a) Order parameters and (b) composition for the I-N_B phase transition for $\kappa_R = 1/\kappa_P = 5$, $\Delta\epsilon = 0$, and $\nu = 1$. Lines without symbols: L2 approximation; lines with symbols: full numerical solution.

(which is equal to the chemical potential) for all three phases vs pressure. We find that N_U^+ and N_U^- have exactly the same Gibbs free energy, which is always less than that of N_B. This is so even for elongation $\kappa_R = 20$, for which one would expect N_B to be stable at high enough density [6]; instead, it is always metastable. The question then naturally arises, Could N_B be stable for yet larger κ_R? To answer it, we calculated the angle-dependent second-virial coefficients in the limit $\kappa \equiv \kappa_R = 1/\kappa_P \to \infty$. In the case considered here, where rods and plates have the same volume $v_0 \equiv v_R = v_P \Rightarrow d_P = d_R\kappa_R^{2/3}$, it is not difficult to show that

$$B_{RR}(\omega_1,\omega_2) = B_{PP}(\omega_1,\omega_2) \approx v_0\kappa^2 \sin^2\theta_{12}, \quad (39)$$

$$B_{RP}(\omega_1,\omega_2) \approx \frac{2\pi}{3}\left(\frac{1}{2}\right)^{3/2} v_0\kappa^{8/3}\cos^2\theta_{12}. \quad (40)$$

It follows that, if κ is very large, the rod-plate excluded volume will be much larger than either the rod-rod or plate-plate excluded volume, which favors a kind of "demixing": at low densities, the system will consist of an isotropic equimolar mixture of rods and plates. As the density is raised, all particles will become either rods or plates, with equal probability, in order to avoid the heavy penalty associated with rod-plate interactions but will remain in the isotropic state; finally, at an even higher density, the rods or plates will order into a uniaxial nematic phase. Thus we do not expect the N_B phase to be stable even in the limit of infinitely long rods and infinitely thin plates.

2. *Biased shapes:* $\Delta\epsilon \neq 0$

For $\Delta\epsilon \neq 0$ we could not find a biaxial phase. If $\Delta\epsilon < 0$ (rods favored), the transition is into the N_U^+ phase (see Fig. 6), whereas if $\Delta\epsilon > 0$ (plates favored), it is into the N_U^- phase (see Fig. 7). As in the case of $\Delta\epsilon = 0$, the N_U^+ phase is rod rich,

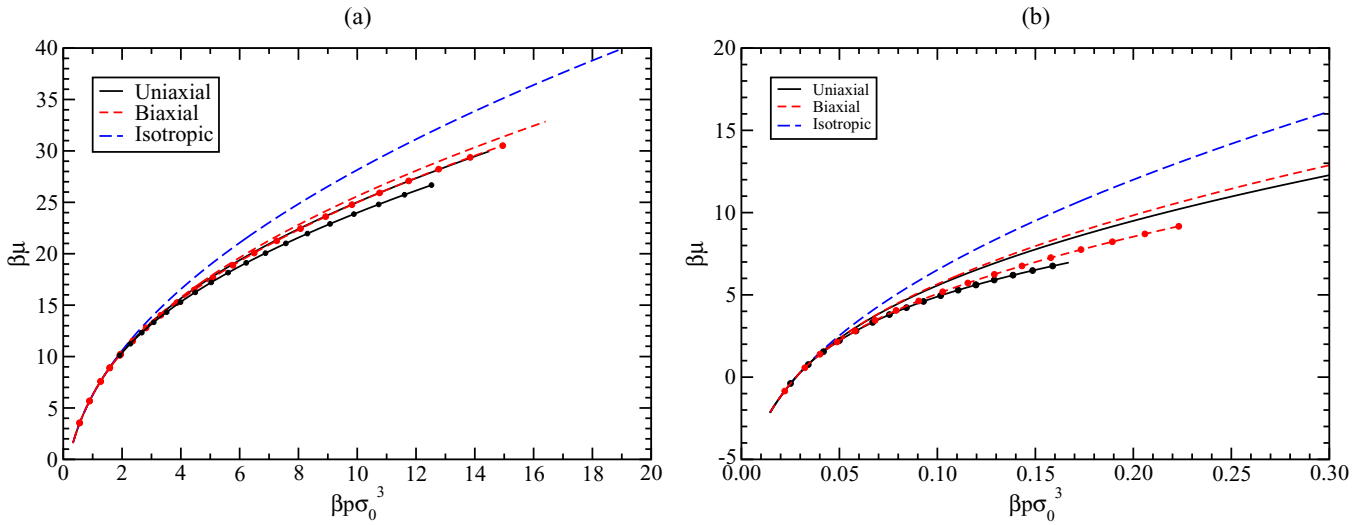

FIG. 5. (Color online) Chemical potential, or Gibbs free energy per particle, of N_U, N_B, and I phases vs pressure for $\Delta\epsilon = 0$, $\nu = 1$ and (a) $\kappa_R = 1/\kappa_P = 5$ and (b) $\kappa_R = 1/\kappa_P = 20$. Lines without symbols: L2 approximation; lines with symbols: full numerical solution.

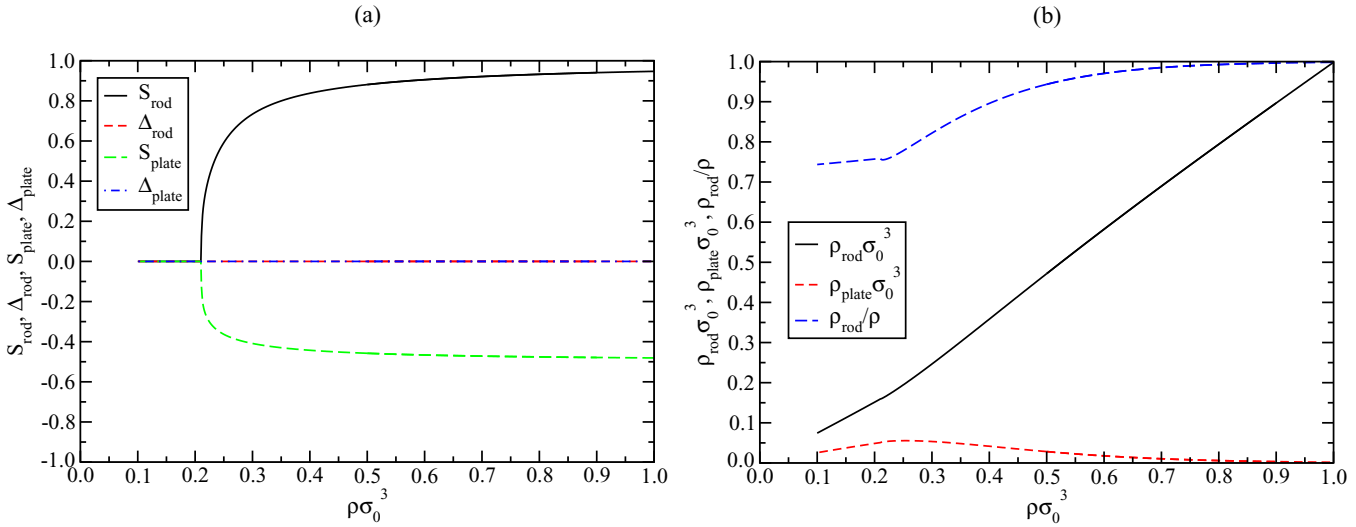

FIG. 6. (Color online) (a) Order parameters and (b) composition for the I-N_U^+ phase transition in the L2 approximation for $\kappa_R = 1/\kappa_P = 5$, $\Delta\epsilon = -1$, and $\nu = 1$.

and the N_U^- phase is plate rich, but now even the I phase is rod rich if $\Delta\epsilon < 0$ and plate rich if $\Delta\epsilon > 0$. This is a result of the intrinsic preference for rods or plates, respectively, regardless of the environment in which they find themselves.

3. *Nonadditive shapes: $\nu \neq 1$*

Here $\Delta\epsilon = 0$ in all cases. As before, we find N_U^+, N_U^-, and N_B phases (Figs. 8, 9, and 10, respectively), depending on our initial guesses for the order parameters. However, if $\nu \gtrsim 1.3$ or $\nu < 1$, the N_B phase is now stable relative to the N_U^+ and N_U^- phases (which again have exactly the same Gibbs free energy; see Fig. 11). Furthermore, for $\nu \gtrsim 1.3$ it is now the N_U^+ (N_U^-) phase that is richer in plates (rods), whereas the N_B phase is again an equimolar mixture of rods and plates. It is also noteworthy that the I-N transition occurs at a lower density than for $\nu = 1$. For $\nu < 1$, on the other hand, the I-N transition is shifted to higher densities, and the N_U^+ (N_U^-) phase is richer in rods (plates), as for $\nu = 1$ (not shown).

Taking $\nu > 1$ means that the rods see the plates as flatter than two plates see each other, and the plates see the rods as longer than two rods see each other. At the same time, the rod-plate excluded volume is greater than it would be for additive particles. The converse is true if $\nu < 1$. It thus appears that, in agreement with earlier work [8,20], shape nonadditivity, of pretty much any kind, promotes biaxiality.

D. Full numerical solution

As noted in Sec. III C, the L2 approximation is known to introduce artifacts owing to its poor representation of the pair excluded volume. In view of the extremely small difference in Gibbs free energies between the N_U and N_B phases, one might reasonably wonder whether the metastability of the N_B phase could be one such artifact. So we went back to solving Eq. (8) using NETLIB routine HYBRD; each iteration of this requires the ODFs, which themselves were found by simple

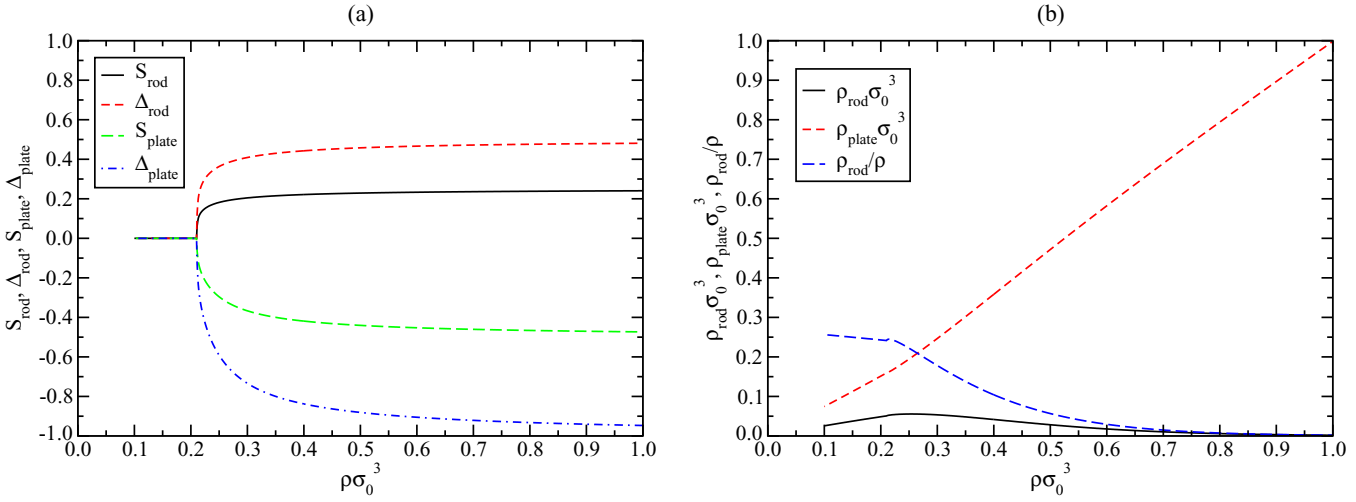

FIG. 7. (Color online) (a) Order parameters and (b) composition for the I-N_U^- phase transition in the L2 approximation for $\kappa_R = 1/\kappa_P = 5$, $\Delta\epsilon = 1$, and $\nu = 1$.

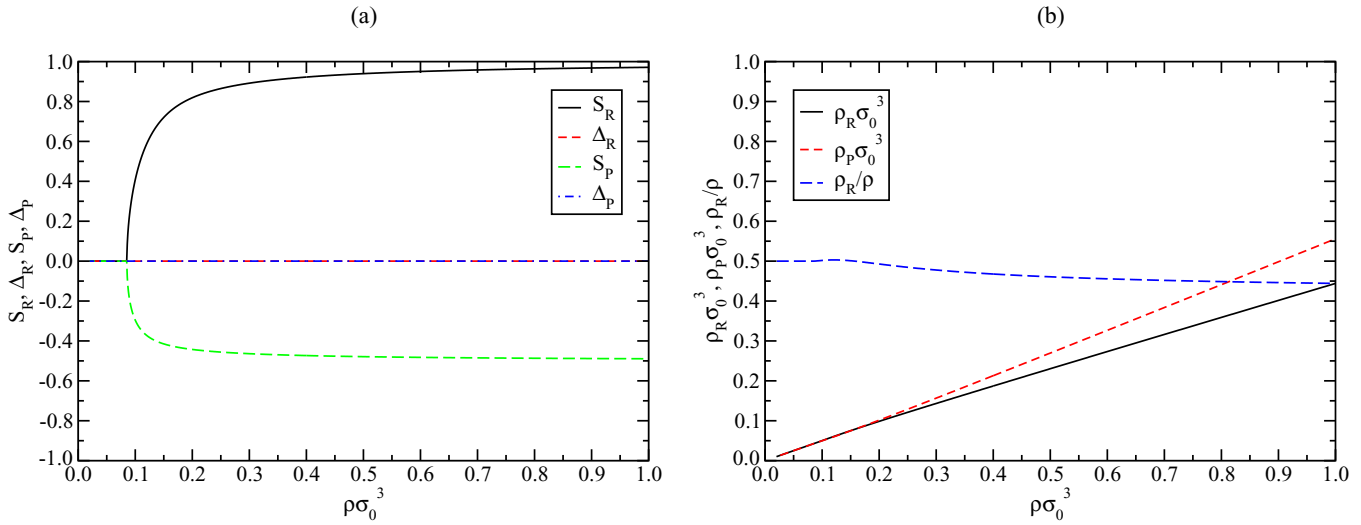

FIG. 8. (Color online) (a) Order parameters and (b) composition for the I-N_U^+ phase transition in the L2 approximation for $\kappa_R = 1/\kappa_P = 5$, $\Delta\epsilon = 0$, and $\nu = 3$.

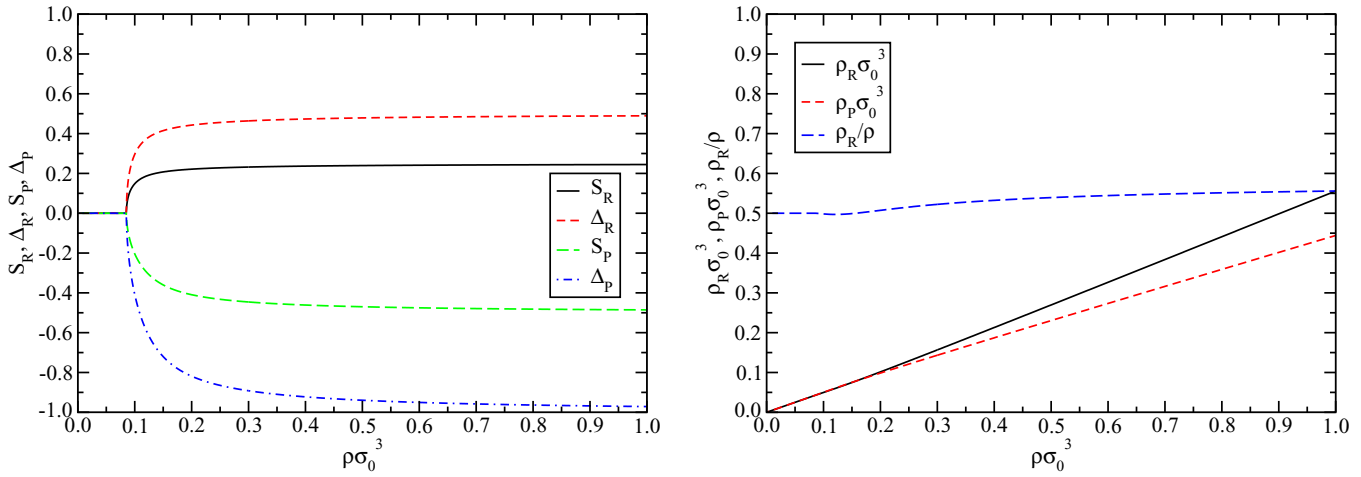

FIG. 9. (Color online) (a) Order parameters and (b) composition for the I-N_U^- phase transition in the L2 approximation for $\kappa_R = 1/\kappa_P = 5$, $\Delta\epsilon = 0$, and $\nu = 3$.

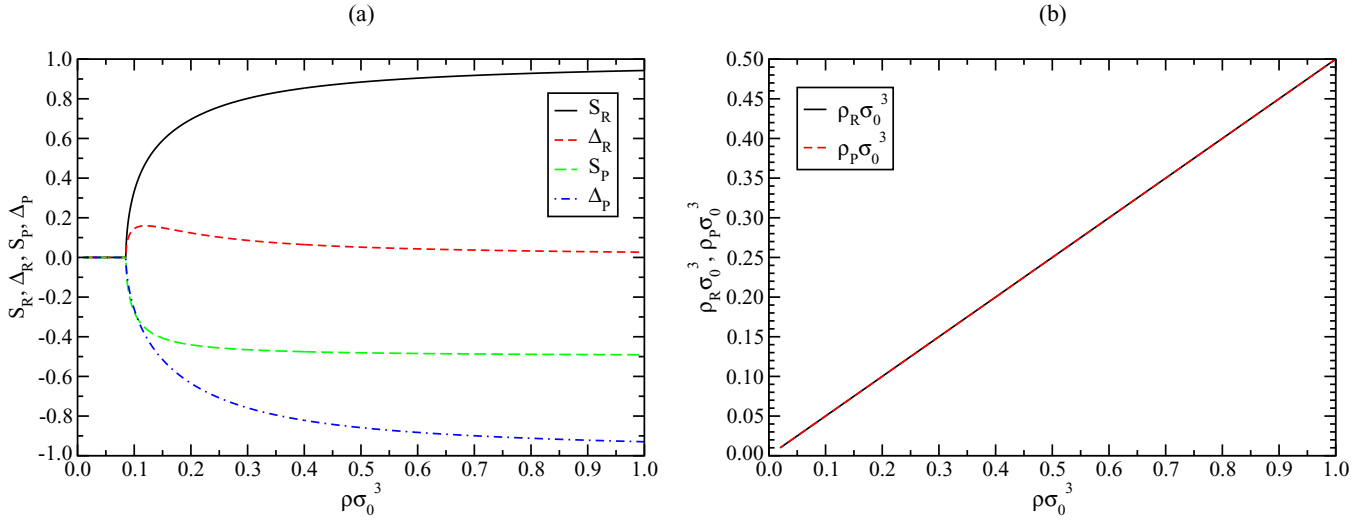

FIG. 10. (Color online) (a) Order parameters and (b) composition for the I-N_B phase transition in the L2 approximation for $\kappa_R = 1/\kappa_P = 5$, $\Delta\epsilon = 0$, and $\nu = 3$.

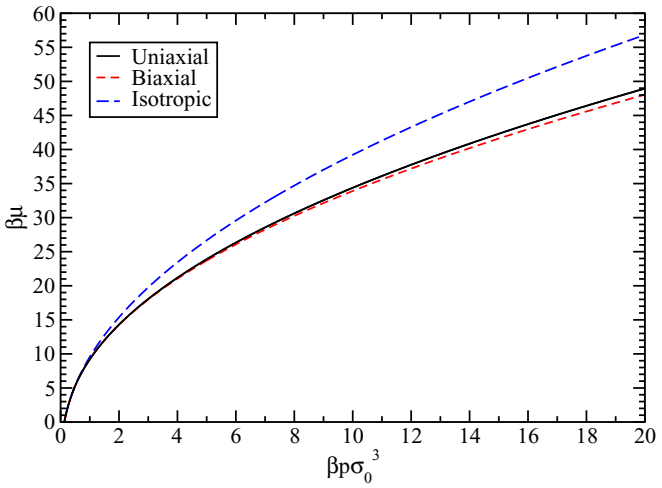

FIG. 11. (Color online) Chemical potential, or Gibbs free energy per particle, of N_U, N_B, and I phases vs pressure in the L2 approximation for $\kappa_R = 1/\kappa_P = 5$, $\Delta\epsilon = 0$. and $v = 3$.

iterative solution of Eqs. (4) and (5). As before, all numerical integrations were performed by 64-point Gauss-Legendre quadrature.

The choice of initial guesses for the ODFs turns out to be crucial: these were taken to be of the form of the L2 ODFs, Eqs. (33) and (34), with guesses made for the rod density and order parameters drawing on Table I of [6]. In all cases we started from deep inside the (uniaxial or biaxial) nematic phase, going down or up in total density. Whereas N_U^+ or N_U^- was easily converged to (see Figs. 2 and 3), the N_B phase required very small density steps and could only be obtained up to densities about 6% higher than that of the transition into the isotropic phase. To circumvent this difficulty, we implemented an alternative, "intermediately numerical" scheme in which we constrained the densities of rods and plates, ρ_R and ρ_P, to be equal and solved only Eqs. (4) and (5). The resulting order parameters coincide with those yielded by the unrestricted numerical solution in the range of densities where both methods can be used, so it is these that we present in Fig. 4(a). If we relax the constraint by allowing ρ_R to be ever so slightly different from ρ_P, the Gibbs free energy goes down: a first hint that the N_B phase is, again, only metastable. And, indeed, this is again borne out by the Gibbs free energy calculations (see Fig. 5; note that the Gibbs free energies of the I phase from the L2 approximation and full numerical solution are the same, as the L2 approximation only affects the orientational part of the free energy).

As announced earlier, the L2 approximation is seen to perform quite well, as it only slightly underestimates the order parameters and the degree of segregation of rods and plates in the N_U^+ and N_U^- phases (see Figs. 2 and 3). This gives us confidence in the conclusions drawn in Secs. III C 2 and III C 3.

IV. DISCUSSION AND CONCLUSIONS

We have studied a minimal model of a mesogen composed of particles that can change shape, which are encountered in some experimental situations. The model consists of interconvertible uniaxial rods and plates, approximated as HGO particles. We considered only rods and plates of the same volume and such that $\kappa_P = 1/\kappa_R$, which implies that all pairs of particles have the same excluded volume. Within Onsager's second-virial theory, we found, from bifurcation analysis as well as from numerical solution of the self-consistent equations, that upon increasing the density the model exhibits a transition from the isotropic to the nematic phase. If there is no energy penalty associated with particle shape change (i.e., $\Delta\epsilon = 0$), the nematic phase can be either rodlike uniaxial (calamitic, N_U^+), platelike uniaxial (discotic, N_U^-), or biaxial (N_B). However, we have verified that, for particle elongations up to $\kappa_R = 20$, the biaxial nematic phase is always metastable with respect to either uniaxial nematic phase. Furthermore, on the basis of an asymptotic calculation, we expect that, in the limit $\kappa \to \infty$, the system will become unstable with respect to either pure rods or pure plates, which obviously do not order biaxially. If, on the other hand, there is a moderate penalty for changing shape (i.e., $\Delta\epsilon \neq 0$), the transition is always from the isotropic into one of the uniaxial nematic phases. Still, we have not considered any other possible competing phases, such as smectics of crystals, which may be more stable at higher densities. We also note that the Gibbs free energy differences between N_U and N_B phases close to the I-N transition are extremely small; hence it might be possible to observe a biaxial nematic phase, even if only metastable.

In summary, although oblate and prolate spheroid mixtures appear to show a biaxial nematic phase [6], our Onsager calculations indicate that such a phase is unstable for interconverting particles, even with no internal energy difference between the oblate and prolate shapes. It would appear that the system can always lower its free energy by breaking the symmetry to form a rod-rich or plate-rich uniaxial nematic phase instead. However, this may be a consequence of the very high symmetry of the particular realization of the model that we have used, namely, the fact that rods and plates have the same volume and all rod-rod and plate-plate pairs have the same excluded volume. Nor have we explored more extreme values of $|\Delta\epsilon| \gg 1$.

As found earlier by others, the biaxial nematic phase can be stabilized by allowing nonadditive particle shapes. Although this may not be easy to realize in experimental systems, it certainly is amenable to computer simulation. The Onsager second-virial approach is known to yield poor quantitative agreement with simulations for small particle elongations, so the theory would need to be modified to incorporate, e.g., Parsons-Lee rescaling [18,23], which has been shown to lead to substantial improvement [6,9–11,17]. In the case of HGOs there is the additional problem that the volume of one particle, and hence the packing fraction, is undefined. Another possible avenue for further research is to consider the effects of third- or higher-order virial coefficients. At this level of approximation the rod-plate symmetry is broken, which may also have implications for the behavior of our model for $\Delta\epsilon = 0$.

ACKNOWLEDGMENTS

P. I. C. Teixeira acknowledges Instituto Superior de Engenharia de Lisboa for sabbatical leave, Fundação para a Ciência e a Tecnologia (Portugal) for financial support through Contracts No. EXCL/FIS-NAN/0083/2012 and No.

UID/FIS/00618/2013, The Isaac Newton Institute, Cambridge (United Kingdom), for support through a Visiting Fellowship, and COST Action MP1305 for partial support.

APPENDIX A: THE EXCLUDED VOLUME OF TWO UNLIKE HGOS

To calculate the orientation dependent second-virial coefficient for dissimilar HGO particles, we refer to Eq. (25) of [14], which we write in the form

$$f_{1/2}(\hat{\mathbf{u}}_1,\hat{\mathbf{u}}_2,\hat{\mathbf{r}}_{12}) = \frac{1}{4\Delta}(1+\hat{\mathbf{r}}_{12}\cdot\mathbf{A}\cdot\hat{\mathbf{r}}_{12}), \tag{A1}$$

where

$$\Delta = \tfrac{1}{2}\left(b_1^2+b_2^2\right), \tag{A2}$$

with $b_i = d_k/2$ being the degenerate transverse semiaxis of particle k ($k=1,2$). The symmetric matrix $\mathbf{A}$ is given by

$$\mathbf{A} = \frac{c_x\hat{\mathbf{u}}_1\hat{\mathbf{u}}_1 + c_y\hat{\mathbf{u}}_2\hat{\mathbf{u}}_2 + c_xc_y(\hat{\mathbf{u}}_1\cdot\hat{\mathbf{u}}_2)(\hat{\mathbf{u}}_1\hat{\mathbf{u}}_2+\hat{\mathbf{u}}_2\hat{\mathbf{u}}_1)}{1+c_xc_y(\hat{\mathbf{u}}_1\cdot\hat{\mathbf{u}}_2)^2}. \tag{A3}$$

There was a typographical error involving a missing factor of 2 in the original equation, and that has been corrected here. As before, $\hat{\mathbf{u}}_1$ and $\hat{\mathbf{u}}_2$ are unit vectors along the symmetry axes of particles 1 and 2, respectively, and $\hat{\mathbf{r}}_{12}$ is the unit vector along the line joining the particle centers. The other symbols in these expressions are given in the main text and depend on the sizes and shapes of the two particles but do not depend on orientation.

The contact distance between the two particles, $\sigma(\hat{\mathbf{r}}_{12},\omega_1,\omega_2)$, is given by Eq. (24) of Ref. [14],

$$\sigma(\hat{\mathbf{r}}_{12},\omega_1,\omega_2) \equiv \sigma(\hat{\mathbf{u}}_1,\hat{\mathbf{u}}_2,\hat{\mathbf{r}}_{12}) = \frac{1}{\sqrt{f_{1/2}(\hat{\mathbf{u}}_1,\hat{\mathbf{u}}_2,\hat{\mathbf{r}}_{12})}}, \tag{A4}$$

and the pair excluded volume is then given by

$$B_2(\hat{\mathbf{u}}_1,\hat{\mathbf{u}}_2) = \frac{1}{6}\int[\sigma(\hat{\mathbf{u}}_1,\hat{\mathbf{u}}_2,\hat{\mathbf{r}}_{12})]^3 d\hat{\mathbf{r}}_{12}. \tag{A5}$$

In order to do this integral it is convenient to write $\mathbf{A}$ in the diagonal form,

$$\mathbf{A} = \lambda_1\hat{\mathbf{e}}_1\hat{\mathbf{e}}_1 + \lambda_2\hat{\mathbf{e}}_2\hat{\mathbf{e}}_2, \tag{A6}$$

where $\hat{\mathbf{e}}_1$ and $\hat{\mathbf{e}}_2$ are orthogonal unit vectors, each being a linear combination of $\hat{\mathbf{u}}_1$ and $\hat{\mathbf{u}}_2$. To obtain these eigenvectors and the corresponding eigenvalues, we need to solve

$$\mathbf{A}\cdot\hat{\mathbf{e}} = \lambda\hat{\mathbf{e}}, \tag{A7}$$

where

$$\hat{\mathbf{e}} = \alpha\hat{\mathbf{u}}_1 + \beta\hat{\mathbf{u}}_2. \tag{A8}$$

This leads to the eigenvalue equation

$$\begin{bmatrix} \hat{\mathbf{u}}_1\cdot\mathbf{A}\cdot\hat{\mathbf{u}}_1-\lambda & \hat{\mathbf{u}}_1\cdot\mathbf{A}\cdot\hat{\mathbf{u}}_2 \\ \hat{\mathbf{u}}_2\cdot\mathbf{A}\cdot\hat{\mathbf{u}}_1 & \hat{\mathbf{u}}_2\cdot\mathbf{A}\cdot\hat{\mathbf{u}}_2-\lambda \end{bmatrix}\begin{bmatrix}\alpha\\ \beta\end{bmatrix} = \begin{bmatrix}0\\0\end{bmatrix}, \tag{A9}$$

where the two eigenvalues are λ_1 and λ_2, as required in Eq. (A6). The corresponding values of α and β may be substituted into Eq. (A8), and this, after normalization, gives the eigenvectors $\hat{\mathbf{e}}_1$ and $\hat{\mathbf{e}}_2$.

We now take $\hat{\mathbf{e}}_1$ to be the z axis and $\hat{\mathbf{e}}_2$ to be the x axis and use polar coordinates, so that the expression for the pair excluded volume becomes

$$B_2(\hat{\mathbf{u}}_1,\hat{\mathbf{u}}_2) = \frac{(4\Delta)^{3/2}}{6}\int_0^{2\pi}d\phi\int_0^{\pi}\sin\theta\,d\theta \times\left(\frac{1}{1+\lambda_1\cos^2\theta+\lambda_2\sin^2\theta\cos^2\phi}\right)^{3/2}, \tag{A10}$$

which may then be evaluated by standard means.

APPENDIX B: BIFURCATION ANALYSIS

This appendix sketches how Mulder's methodology [21] may be applied to the problem of shape-changing spheroids, first, to calculate the density $\rho^{(0)}$ at which the isotropic phase first becomes unstable with respect to nematic fluctuations and, second, to find out what conditions are necessary for a continuous transition. This could be either to a biaxial nematic phase N_B, or to coexisting N_U^+ and N_U^- phases.

We write

$$\rho = \rho^{(0)} + \varepsilon\rho^{(1)} + \varepsilon^2\rho^{(2)} + \cdots, \tag{B1}$$

$$\hat{f}_{R,P}(\omega) = \hat{f}^{(0)}_{R,P}(\omega) + \varepsilon\hat{f}^{(1)}_{R,P}(\omega) + \varepsilon^2\hat{f}^{(2)}_{R,P}(\omega) + \cdots, \tag{B2}$$

where $\hat{f}^{(0)}_{R,P}(\omega) = 1/4\pi$, the ODFs for rods and plates in the isotropic phase. As discussed in [21], we are free to choose the higher-order terms in Eq. (B2) to be orthogonal to $\hat{f}^{(0)}_{R,P}(\omega)$. In this case, this means that the integral of each of the higher-order terms is zero.

The rod and plate ODFs satisfy Eqs. (4) and (5), and we also have the equal chemical potential condition,

$$\mu_R = \mu_P, \tag{B3}$$

where the chemical potentials of rods and plates are given by Eqs. (2) and (3), respectively. We seek solutions as a power series in ε.

To order ε^0, we have an isotropic phase at an overall density $\rho^{(0)}$ and where the rod and plate densities are given by the isotropic solution of Eq. (B3). We denote the corresponding mole fractions as $x^{(0)}_{R,P}$. For the important special case where $\Delta\epsilon = 0$, we have $x^{(0)}_R = x^{(0)}_P = 0.5$.

To determine the value of the bifurcation density $\rho^{(0)}$, we consider the $O(\varepsilon)$ solution. Equation (B3) shows there to be no first-order correction to the isotropic mole fractions, i.e., $x^{(1)}_R = x^{(1)}_P = 0$. Equations (4) and (5) yield

$$\hat{f}^{(1)}_R(\omega) = -2\rho^{(0)}\left[x^{(0)}_R\int B_{RR}(\omega,\omega')\hat{f}^{(1)}_R(\omega')\,d\omega' + x^{(0)}_P\int B_{RP}(\omega,\omega')\hat{f}^{(1)}_P(\omega')\,d\omega'\right], \tag{B4}$$

$$\hat{f}^{(1)}_P(\omega) = -2\rho^{(0)}\left[x^{(0)}_R\int B_{RP}(\omega,\omega')\hat{f}^{(1)}_R(\omega')\,d\omega' + x^{(0)}_P\int B_{PP}(\omega,\omega')\hat{f}_P(\omega')\,d\omega'\right], \tag{B5}$$

i.e., a set of eigenfunction equations for $\hat{f}^{(1)}_{R,P}(\omega)$. As discussed in [21], the relevant degenerate solution is spanned by the set

of second-rank spherical harmonics. If this form of solution is substituted into Eqs. (B4) and (B5) and use is made of Eqs. (28) and (29) in the main text, one ends up with a standard algebraic eigenvalue equation. The solution of this yields the bifurcation density, as given in Eq. (27) using a slightly different, but hopefully obvious, notation.

This first-order analysis, however, provides no information about the nature of the nematic instability or whether the transition is first order or continuous. To obtain this information, we need to go to second order in ε. This is a little intricate but essentially follows the clear exposition given in [21] with just a few technical differences.

We start by noting that second-order changes to the rod and plate mole fractions, as determined by Eq. (B3), play no role in the second-order equations for the ODFs. Thus the rod and plate mole fractions are the same as above.

The second-order analysis follows the techniques of degenerate perturbation theory. The second-order equation for the rod ODF is

$$\begin{aligned}\hat{f}_R^{(2)}(\omega) = &-2\rho^{(0)}\left[x_R^{(0)}\int B_{RR}(\omega,\omega')\hat{f}_R^{(2)}(\omega')\,d\omega' + x_P^{(0)}\int B_{RP}(\omega,\omega')\hat{f}_P^{(2)}(\omega')\,d\omega'\right]\\ &+2[\rho^{(0)}]^2\left\{\left[x_R^{(0)}\int B_{RR}(\omega,\omega')\hat{f}_R^{(1)}(\omega')\,d\omega'\right]^2 + \left[x_P^{(0)}\int B_{RP}(\omega,\omega')\hat{f}_P^{(1)}(\omega')\,d\omega'\right]^2\right\}\\ &-2\rho^{(1)}\left[x_R^{(0)}\int B_{RR}(\omega,\omega')\hat{f}_R^{(1)}(\omega')\,d\omega' + x_P^{(0)}\int B_{RP}(\omega,\omega')\hat{f}_P^{(1)}(\omega')\,d\omega'\right]\\ &-2[\rho^{(0)}]^2\int\left\{\left[x_R^{(0)}\int B_{RR}(\omega,\omega')\hat{f}_R^{(1)}(\omega')\,d\omega'\right]^2 + \left[x_P^{(0)}\int B_{RP}(\omega,\omega')\hat{f}_P^{(1)}(\omega')\,d\omega'\right]^2\right\}d\omega, \qquad \text{(B6)}\end{aligned}$$

and there is a similar expression for the plate ODF.

The first-order distribution functions are written as linear combinations of second-rank spherical harmonics, e.g.,

$$\hat{f}_R^{(1)}(\omega) = \mathcal{A}_{0,R}Y_0^2(\omega) + \frac{\mathcal{A}_{2,R}}{\sqrt{2}}\left[Y_2^2(\omega) + Y_{-2}^2(\omega)\right], \qquad \text{(B7)}$$

and a similar expression exists for the plates. If one multiplies Eq. (B6) and the equivalent expression for plates by each eigenfunction in Eq. (B7) and then integrates over angles, one first eliminates the unknown second-order ODFs, and second, one obtains expressions for the $\mathcal{A}$ coefficients (two for the rod ODF and two for the plate ODF). Details are given in [21].

Finally, again as argued in [21], the transition is continuous when $\rho^{(1)} = 0$. Imposing this condition gives Eq. (32). As noted previously, this condition may correspond either to a continuous isotropic-biaxial nematic transition or to a continuous transition from isotropic to two coexisting nematic phases.

[1] K. Merkel, A. Kocot, J. K. Vij, R. Korlacki, G. H. Mehl, and T. Meyer, Phys. Rev. Lett. **93**, 237801 (2004).

[2] J. L. Figueirinhas, C. Cruz, D. Filip, G. Feio, A. C. Ribeiro, Y. Frère, T. Meyer, and G. H. Mehl, Phys. Rev. Lett. **94**, 107802 (2005).

[3] A. F. Terzis, A. G. Vanakaras, and D. J. Photinos, Mol. Cryst. Liq. Cryst. Sci. Technol., Sect. A **352**, 265 (2000).

[4] A. G. Vanakaras, A. F. Terzis, and D. J. Photinos, Mol. Cryst. Liq. Cryst. Sci. Technol., Sect. A **362**, 67 (2001).

[5] M. V. Gorkunov, M. A. Osipov, A. Kocot, and J. K. Vij, Phys. Rev. E **81**, 061702 (2010).

[6] P. J. Camp, M. P. Allen, P. G. Bolhuis, and D. Frenkel, J. Chem. Phys. **106**, 9270 (1997).

[7] R. van Roij and B. Mulder, J. Phys. II **4**, 1763 (1994).

[8] S. Varga, A. Galindo, and G. Jackson, Phys. Rev. E **66**, 011707 (2002).

[9] S. Varga, A. Galindo, and G. Jackson, J. Chem. Phys. **117**, 7207 (2002).

[10] S. Varga, A. Galindo, and G. Jackson, J. Chem. Phys. **117**, 10412 (2002).

[11] A. Galindo, A. J. Haslam, S. Varga, G. Jackson, A. G. Vanakaras, D. J. Photinos, and D. A. Dunmur, J. Chem. Phys. **119**, 5216 (2003).

[12] M. Rigby, Mol. Phys. **68**, 687 (1989).

[13] B. J. Berne and P. Pechukas, J. Chem. Phys. **56**, 4213 (1972).

[14] D. J. Cleaver, C. M. Care, M. P. Allen, and M. P. Neal, Phys. Rev. E **54**, 559 (1996).

[15] J. W. Perram and M. S. Wertheim, J. Comput. Phys. **58**, 409 (1985); J. W. Perram, J. Rasmussen, E. Praestgaard, and J. L. Lebowitz, Phys. Rev. E **54**, 6565 (1996).

[16] M. P. Allen, G. T. Evans, D. Frenkel, and B. M. Mulder, Adv. Chem. Phys. **86**, 1 (1993).

[17] P. Padilla and E. Velasco, J. Chem. Phys. **106**, 10299 (1997).

[18] J. D. Parsons, Phys. Rev. A **19**, 1225 (1979).

[19] This was suggested by D. J. Cleaver.

[20] A. Chrzanowska, Phys. Rev. E **58**, 3229 (1998).

[21] B. Mulder, Phys. Rev. A **39**, 360 (1989).

[22] A. Stroobants and H. N. W. Lekkerkerker, J. Phys. Chem. **88**, 3669 (1984).

[23] S. D. Lee, J. Chem. Phys. **87**, 4972 (1987).